

5 Results and Discussions

5.1 Introduction

In this chapter, we present the results of this project. More specifically, we will present the fabricated devices and their measured performance.

As mentioned in the introduction chapter, the wireless headstages are usually mounted on the animal head in a surgery procedure. In our case, the final headstage consists of two parts: a removable part and a non-removable part. The non-removable part will be mounted on the animal head permanently while the removable part can be placed on or removed from the non-removable part using a board-to-board connector from Molex Inc. [99].

The non-removable part of the headstage is not the goal of this project and is provided by other research groups. It has the appropriate physical shape to be mounted on the animal head and it consists of the LEDs and the electrodes that will be placed in the animal head. The terminals of these LEDs and electrodes will be connected to the board-to-board connector of the non-removable part. The removable part will have a matching connector that will interface to the LEDs/electrodes terminals.

In order to realize the removable part of the headstage system, two PCBs have been designed which can carry the headstage components. One PCB has been designed as a prototype and has larger dimensions than the headstage requirements. The other PCB has the required dimensions of the headstage and is fabricated using the rigid-flex PCB manufacturing technology. The rigid-flex characteristics of the (final) headstage PCB results in low volume and higher robustness to EMC/EMI issues.

Only the prototype PCB has been fabricated and tested at the time of this writing, and the other PCB has been sent for fabrication. All tests that are mentioned in this chapter have been carried out on the prototype PCB. From this point, we will refer to the removable part of the headstage, as *headstage*.

5.2 Headstage PCBs and Their Specifications

In this section, we present the two designed PCBs and their specifications.

5.2.1 Prototype PCB

The fabricated prototype PCB[†] is a 4-layer PCB having 2 signal layers and 2 power planes. It has all the components that will be mounted on the PCB including the LEDs and the electrodes but its size is intentionally

[†] This PCB has been mainly designed by Gabriel Gagnon-Turcotte and was edited by Reza Ameli and Alireza Avakh Kisomi.

more than the targeted headstage size so it would be easy to debug. This PCB measures 102×54.2 mm² and it has 485 pads, 2573 tracks and 114 vias. The minimum track width/spacing is 0.2 mm and the minimum hole diameter is 0.4 mm. The layer stacking of this PCB is shown in Table 10.

Table 10. Headstage prototype PCB layer stack.

Layer	Type
1	Signal
2	VDD 3.3 v
3	GND
4	Signal

This PCB has been designed larger than the headstage size requirements so it would be easier to solder SMD components and debug. Figure 20 shows the fabricated *prototype* PCB, Figure 21 shows the 2D PCB layout, Figure 22 shows the front view of the 3D PCB layout and Figure 23 shows the back view of the 3D PCB layout.

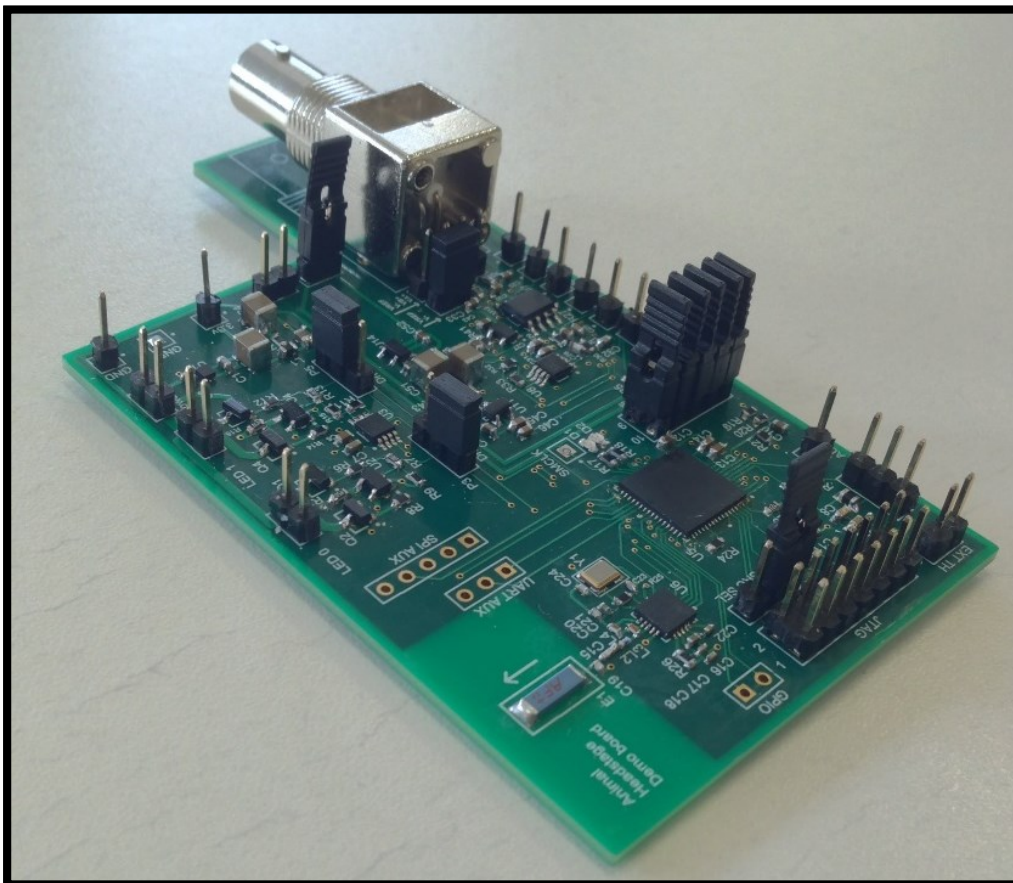


Figure 20. Fabricated headstage prototype PCB.

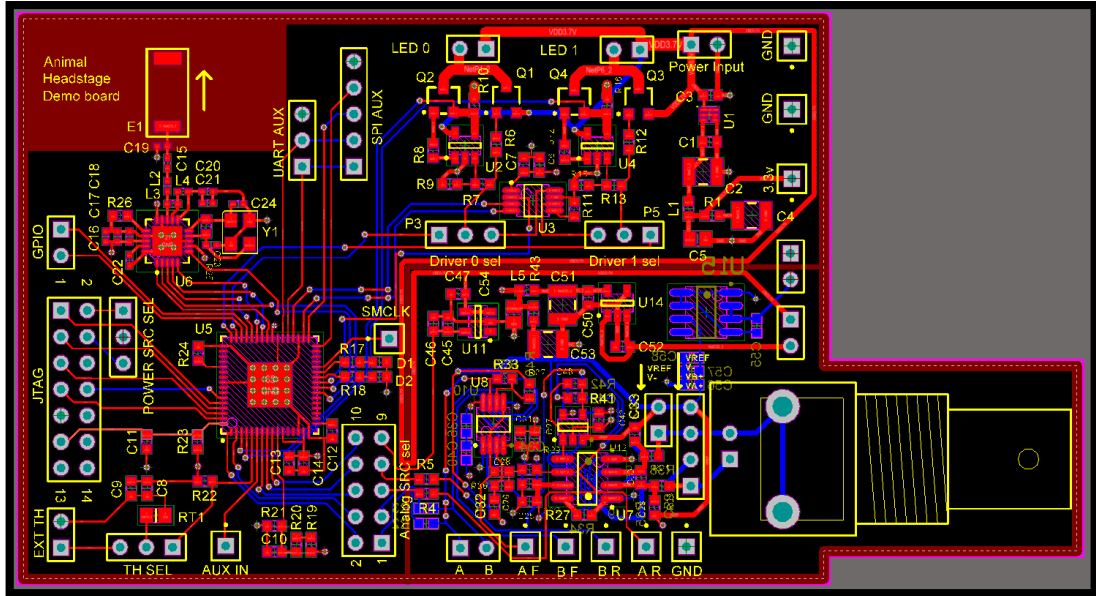


Figure 21. Headstage prototype PCB (2D view).

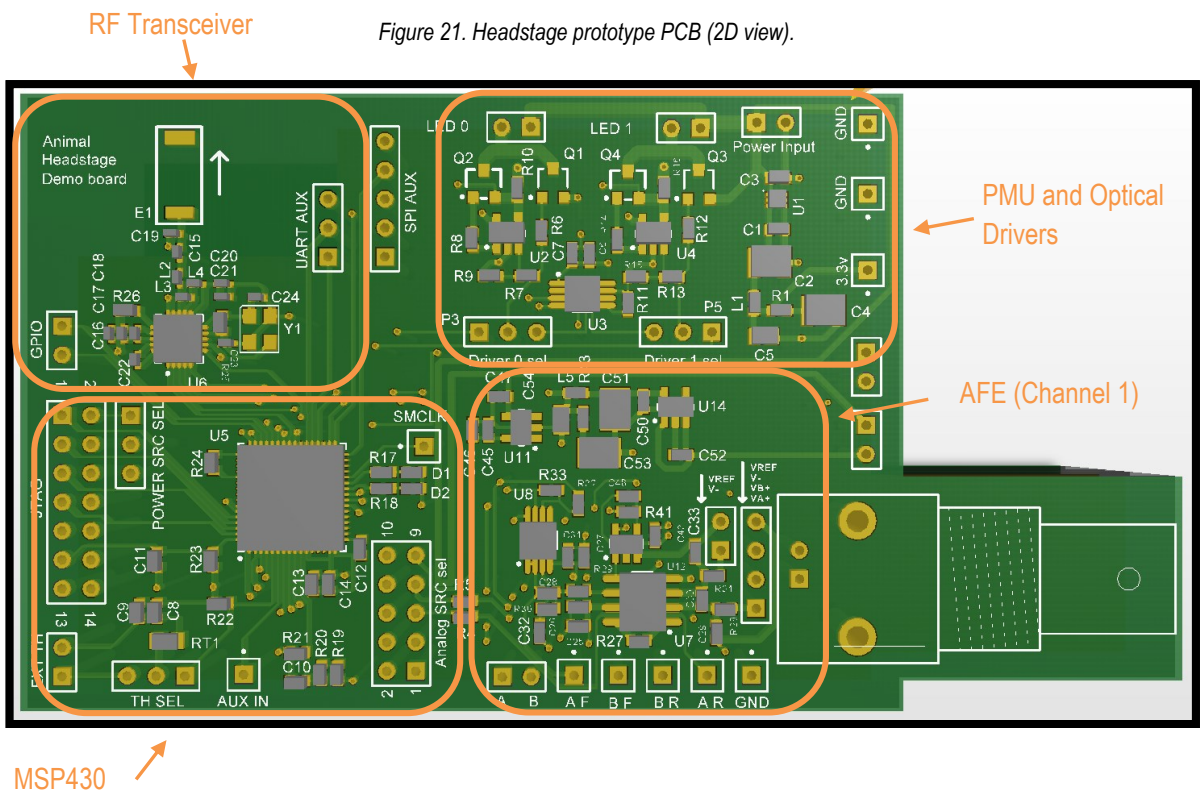


Figure 22. Headstage prototype PCB, front view (3D).

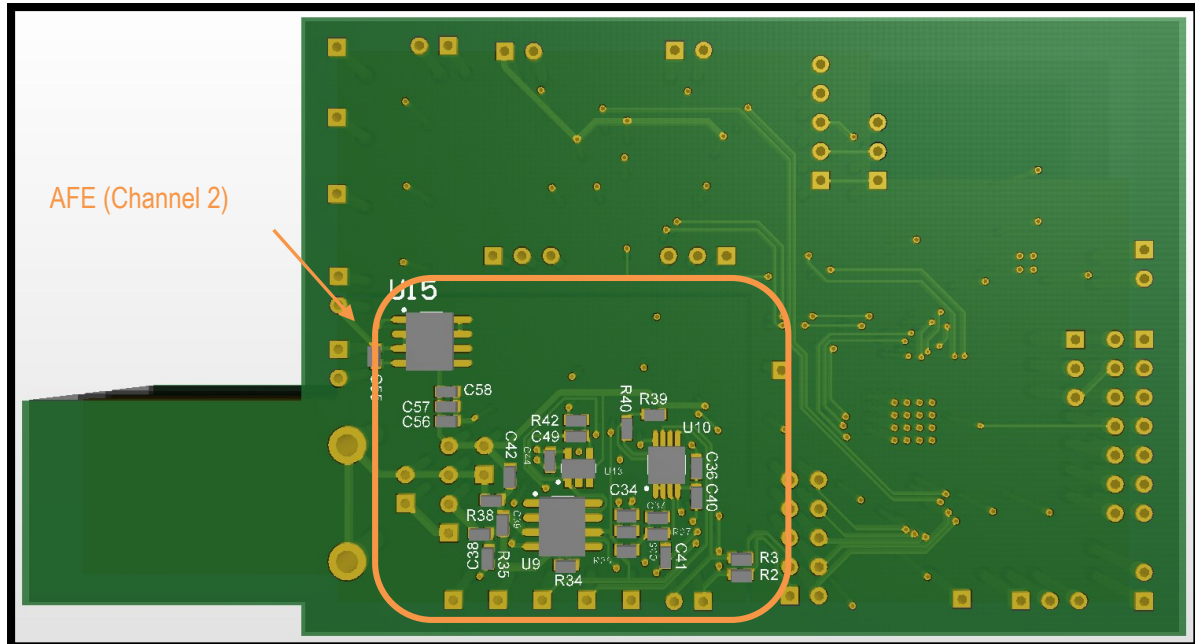


Figure 23. Headstage prototype PCB, back view (3D).

As mentioned before, the prototype PCB has been designed to help with testing and debugging the headstage circuits. It has one BNC connector that can be used to inject signals to the system with minimal added noise. We have tried to use the electronic components that will be used for the final version of the headstage on the prototype as much as possible.

5.2.1.1 EMC/EMI Considerations

In order to ensure the correct functionality of this prototype system, the following EMC/EMI techniques have been used:

- 1) The power plane and the ground plane are divided into two sections. One section is dedicated to the AFE while the other section is dedicated to all other subsystems of the headstage. This technique ensures that the current return paths of the signals that are not analog will not share the power/ground plane with the AFE. It should be noted that separating power/ground planes means that the plane is divided in two sections that are connected to each other only at a small connection point [97].
- 2) All digital high-speed traces have ground plane beneath them. This technique assures that the electromagnetic emissions of the high-speed digital signals will be cancelled out by the electromagnetic emissions of their return currents. As a result, the noise that will be picked up by other conductors will be minimum.
- 3) All traces have power/ground planes. This results into minimum noise picked up by any conductor.

- 4) Components with high CMRR/PSRR have been used. Also, power supply filters have been incorporated. For more details please refer to Chapter 4.

The prototype PCB has been fully tested and satisfies all the design requirements. All the measured results are presented in the results section in this chapter.

5.2.2 Final Headstage PCB

The final headstage PCB, being the removable part of the headstage system, has been design on a rigid-flex PCB with 6 layers. However this PCB has not been fabricated yet. This PCB will carry the same parts that are mounted on the prototype PCB (except for the LEDs and the electrodes) but has the required form factor of the final headstage. As mentioned in the introduction of this chapter, the final headstage PCB is fabricated using the rigid-flex technology resulting in less occupied volume and better EMC/EMI robustness.

The final headstage PCB measures $65 \times 20.9 \text{ mm}^2$ when unrolled, has minimum trace width/spacing of 0.2 mm and the minimum hole diameter is 0.2 mm. Table 11 shows the layer stacking of this PCB.

Table 11. Final headstage PCB layer stack.

Layer	Type
1	Signal
2	Power
3	Signal
4	Signal
5	GND
6	Signal

The rationale behind this stacking is that most PCB manufacturers prefer to have signal layers as the inner layers when fabricating rigid-flex PCBs.

This rigid-flex PCB has 3 rigid sections that are connected to each other using the flexible sections. This design strategy eliminates the need for bulky board-to-board connectors. Each rigid section measures $15 \times 21 \text{ mm}^2$ and each flexible section measures $10 \times 21 \text{ mm}^2$.

When the rigid parts are folded together, as is the goal of designing this rigid-flex PCB, the headstages measures less than $20 \times 20 \text{ mm}^2$ depending on the folding angle, as stated by the design requirements. Figure 24 shows the unrolled PCB in 2D view.

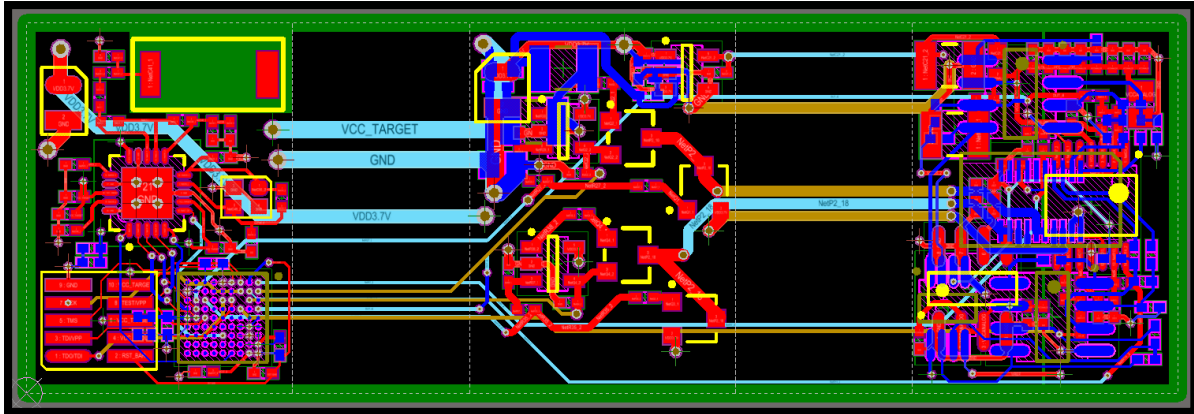


Figure 24. Final headstage PCB unrolled 2D view.

It can be seen that the three rigid parts are connected to each other using light blue and yellow traces. The rigid sections are those populated with components while the flex sections contain only PCB traces. The board-to-board connector is placed on the back of the rigid section at the right side of Figure 24. In Figure 25 and Figure 26, we can see the top view, bottom view and the unrolled final headstage PCB. More specifically, on the right-hand side of Figure 25, the white board-to-board connector can be seen.

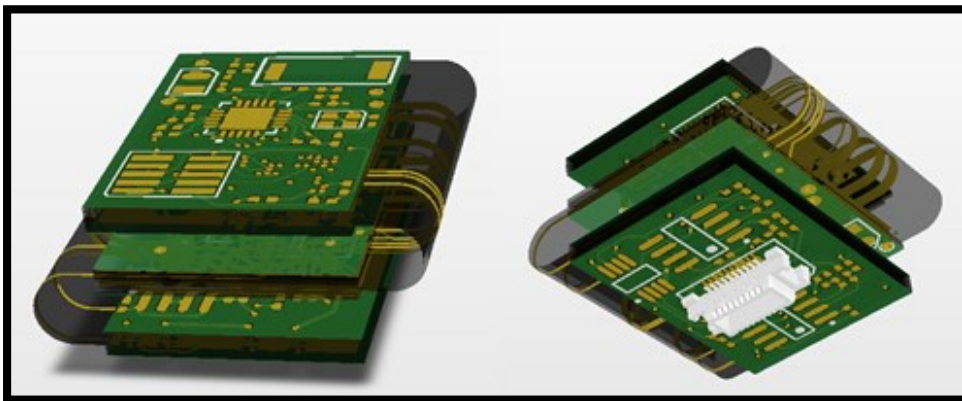


Figure 25. Left: final PCB headstage rolled (top view). Right: final PCB headstage rolled (bottom view).

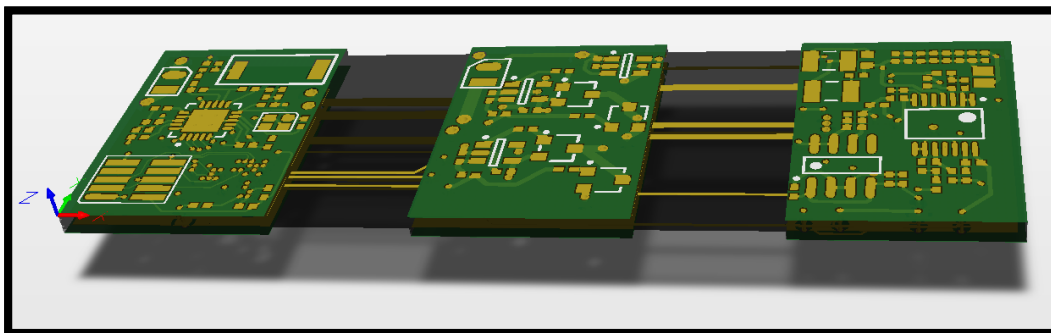


Figure 26. Final PCB headstage unrolled.

While Figure 25 and Figure 26 show the removable part of the headstage system, Figure 27† and Figure 28 show the complete headstage system that will be mounted on the animal head with and without proper packaging. The packaging might be required to protect the headstage from damages caused by animal movements. It can be seen that optical fibers, along with electrodes, will be implemented inside the animal brain.

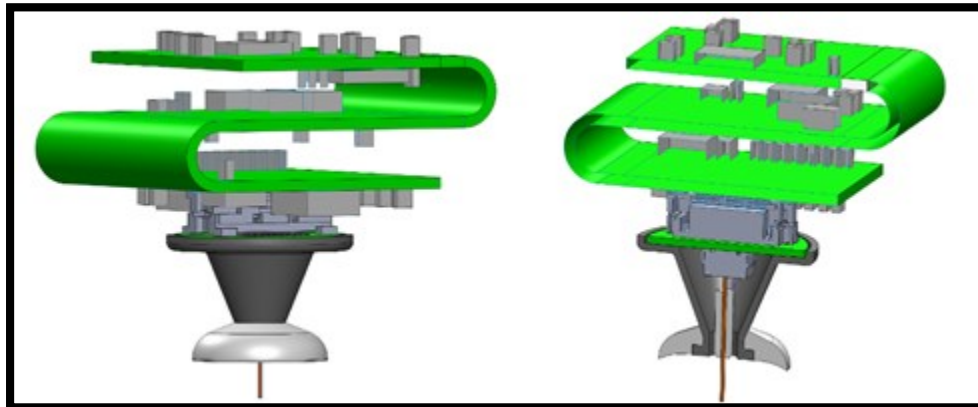


Figure 27. Left: complete headstage system connected to the non-removable part. Right: cross-section view of the complete headstage system.

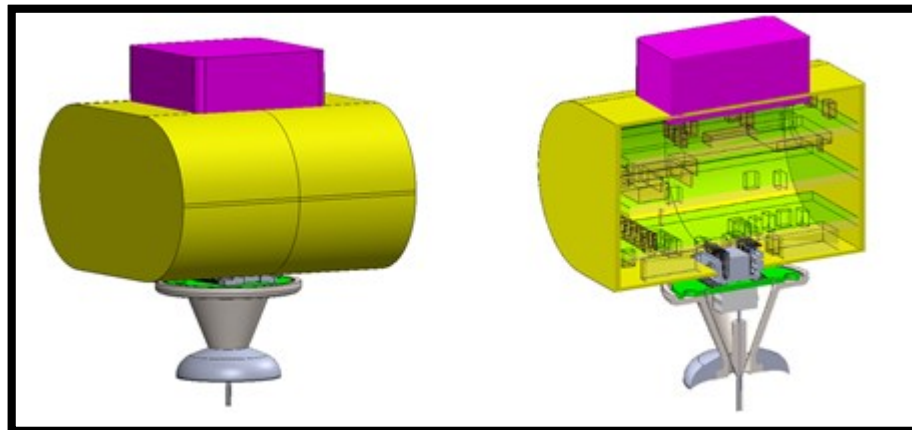


Figure 28. Left: complete headstage system in package. Right: cross-section view of the complete headstage system in package.

5.2.2.1 EMC/EMI Considerations

The EMC/EMI considerations of the final headstage PCB are similar to those of the prototype headstage. However, the final headstage PCB benefits from the inherent separation of different rigid sections. Furthermore, since the rigid section dedicated to the AFE is separate from the other subsystems, more EMC/EMI robustness is resulted.

† Figure 27 and Figure 28 were created by Doric Lenses Inc., Québec, Canada.

5.3 Measured Performance of the AFE

In this section, we present the measured performance of the analog front end (AFE). Three types of test have been carried out to test the AFE. Using these three tests, almost all characteristics of the AFE can be measured.

In the first type of test, the AFE differential inputs have been shorted out together and the noise characteristics of the AFE have been measured. Attention has been paid to the quality of the short circuit as using long wires will result in higher picked up noise. The *input-referred noise* can be calculated by dividing the noise at the AFE output by the overall AFE gain.

In the second type of test, the AFE characteristics including the gain and the cut-off frequencies have been measured using an Agilent 35670A dynamic signal analyzer.

Finally, in the third type of test, synthesized but realistic action potential signals with realistic amplitudes were fed to the AFE and the output of the signal chain (AFE and headstage outputs) were measured.

It should be noted that all the measurements were carried out while the system was working i.e., the LEDs were blinking and the radio was transmitting. In this scenario, all noise sources from other headstage subsystems are present. It can be verified that the high-current LED signals, fast digital signals and the radio RF signals do not affect the performance of the AFE.

Table 12 and Figure 29[†] provide the measurement results provided by the Agilent dynamic signal analyzer. It can be seen that the input-referred noise of the AFE is low enough for action potentials of 10 microvolts to be detected. Moreover, the AFE characteristics conform to those of the design requirements. The measurement results of the synthetic action potentials will be presented in a later subsection in this chapter.

Table 12. Measured AFE characteristics.

Parameter	Value
Gain	2851 V/V (69.09 dB)
Low Cut-Off Frequency	285 Hz
High Cut-Off Frequency	6580 Hz
Input-Referred Noise	2.1 μ V(RMS)
Power Consumption	1 mA @ 3.0 V (3 mW)

[†] This graph has been prepared by Alireza Avakh Kisomi, M.Sc. student at Laval University, 2015.

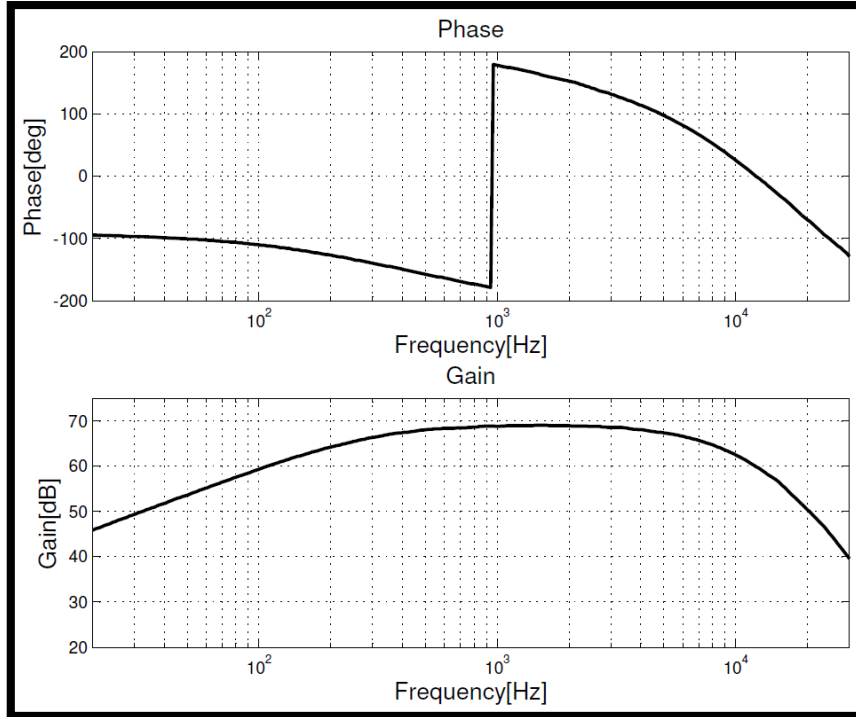


Figure 29. Bode plot of the AFE transfer function.

5.4 Measured Performance of the Optical Stimulation Circuitry

The optical stimulation circuitry has been tested by measuring the voltage on the LED terminals and the current that passes through the LED. The blue LED [87] has been used to carry out the tests. Table 13 summarizes the optical stimulation circuitry performance and Figure 30[†] shows the voltage on the LED terminals. It can be verified that the rise-time/fall-time of the LED stimulation pattern is negligible compared to the pulse length (i.e., when LED is on) and that the pattern is sharp. This fulfills the needs of the optogenetic experiments having millisecond-scale stimulation patterns.

Table 13. Measured characteristics of the optical stimulation circuitry.

Parameter	Value
LED Terminal Voltage when Active	3.275 V
LED Current when Active	150 mA
Stimulation (PWM) Frequency	1 Hz to 100 Hz
Duty Cycle	10%
Rise Time	1.6 μ sec
Fall Time	5.1 μ sec
LED input power	491.25 mW

[†] This screenshot from an oscilloscope has been made by Alireza Avakh Kisomi and Gabriel Gagnon-Turcotte, M.Sc. students at Laval University, 2015.

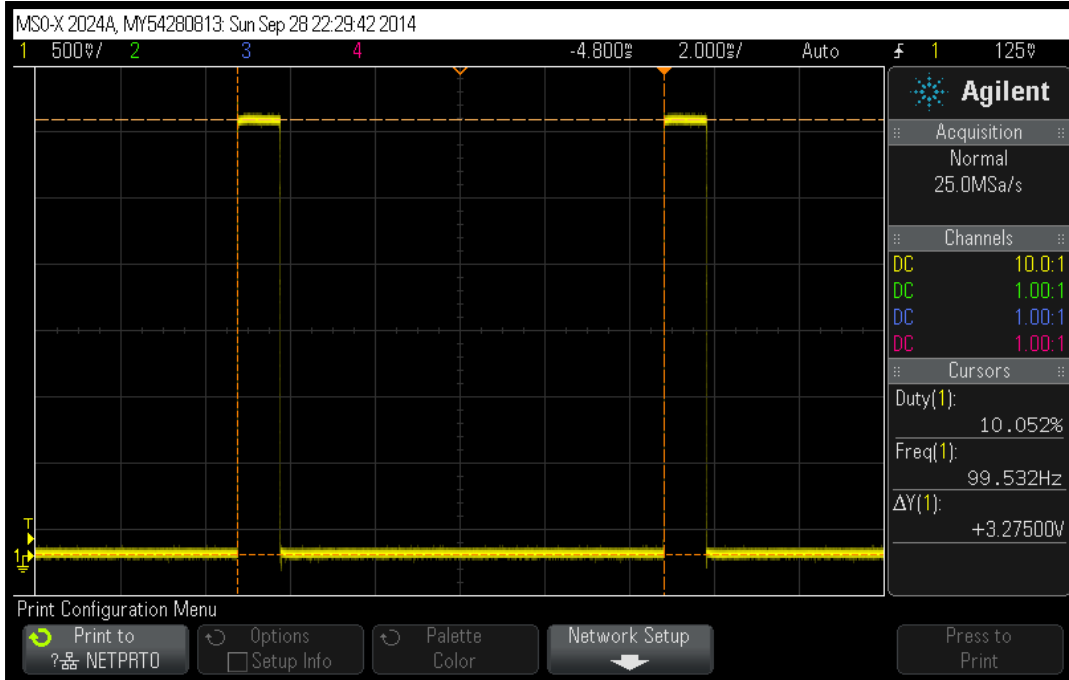


Figure 30. LED voltage during stimulation.

5.5 Power Consumption Measurements

In this section, we present the measured power consumption of all headstage subsystems. The headstage has been powered by a 110 mAh Li-ion battery (GSP061225D2C, Great Power Battery Co., LTD [100]). This battery occupies a volume of $5.7 \times 12 \times 28 \text{ mm}^3$ and has a maximum continuous discharge current of 200 mA. We have chosen this battery as it provides a compromise between size and capacity. Table 14 and Figure 31† provide the power consumption of different headstage subsystems (System LED is a small indication LED used to show the system operation). In our measurements, we have set the stimulation duty cycle to its maximum (10%).

Table 14. Power consumption of headstage subsystems.

Component	Power Consumption When Active
AFE	0.415 mA (1.54 mW)
MCU	4.53 mA (16.8 mW)
Radio Transceiver	4.52 mA (16.7 mW)
Optical Stimulation Circuitry	4.08 mA (15.1 mW)
Stimulation LEDs	15.0 mA (55.5 mW)
System LED	2 mA (7.4 mW)
Total	30.804 mA (113.97 mW)

† This figure has been made by Gabriel Gagnon-Turcotte, M.Sc. student at Laval University, 2015.

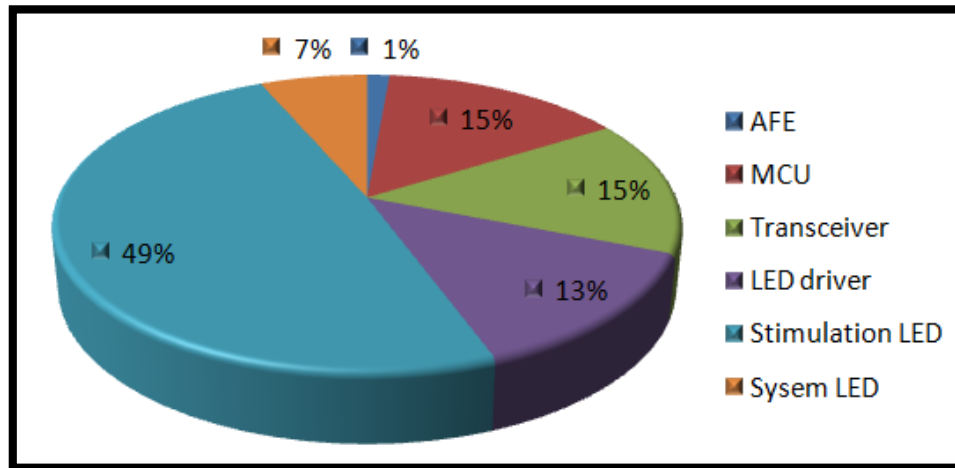


Figure 31. Power consumption of headstage subsystems.

The total average current consumption of the headstage system is 30.804 mA which insures more than 3 hours of continuous lifetime when using a 110 mAh battery as is the case in the headstage system.

5.6 Headstage Outputs with Synthetic Action Potentials as Input

As mentioned in the AFE performance section, one of the tests that have been carried out was feeding the AFE with synthetic but realistic action potentials (these signals have been obtained from the website of authors of [32]). In this section, we will show the outputs of the signal chain when such synthetic signals are fed to the AFE inputs.

Similar to previous tests, this test was carried out when the stimulation LEDs were blinking at their maximum current. In order to realize synthetic action potentials, an arbitrary function generator (Tektronix AFG3101C [101]) has been used. Since the minimum output voltage of this function generator is much larger than the action potential amplitudes, a resistive divider has been used. The resistive divider has been placed in a very close proximity of the AFE input so the picked up noise becomes minimum.

Figure 32[†] and Figure 33 show the many action potentials acquired by the headstage system. It can be verified that the headstage system acquires signals with high fidelity. However, to test the signal acquisition fidelity in a more quantitative manner, a test has been carried out which will be described later in this section. Figure 34 shows the acquired action potentials and a scaled version stimulation pattern (voltage across the 0.5 ohm resistor in the optical stimulation circuitry) in the same graph. It can be seen that the stimulation pattern, requiring high levels of current has no impact on the quality of the acquired signals.

[†] Figure 32, Figure 33 and Figure 34 were created by Gabriel Gagnon-Turcotte, M.Sc. student at Laval University, 2015.

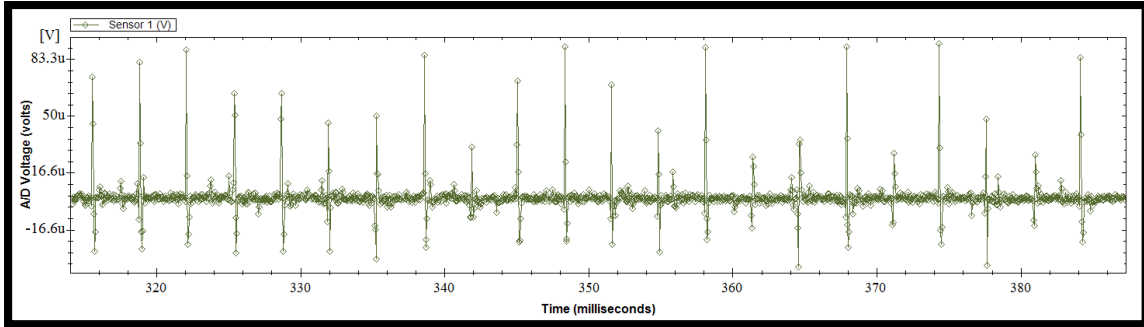


Figure 32. Action potential train acquired by the headstage system.

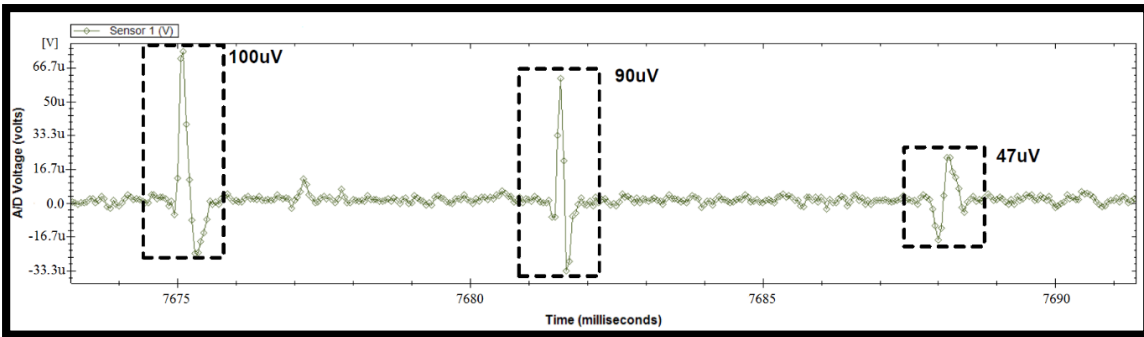


Figure 33. Action potential train acquired by the headstage system (zoomed in).

In order to test the fidelity of the signal acquisition chain, we performed the following test: the 500 action potentials on a 10-second synthetic neural signal were clustered before and after acquisition by the headstage system. We expect that same results yield after the signal is passed through the headstage system. We got the expected results i.e., passing the neural signal through the headstage signal chain has no effect on the shapes of the action potentials. Figure 35[†] shows the clustered signals.

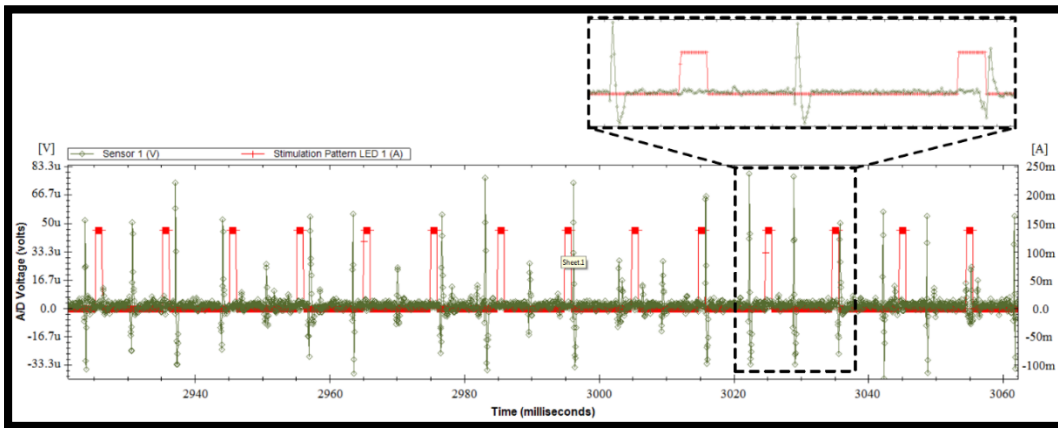


Figure 34. Action potential train acquired by the headstage system along with the stimulation pattern.

[†] This figure was created by Gabriel Gagnon-Turcotte, M.Sc. student at Laval University, 2015.

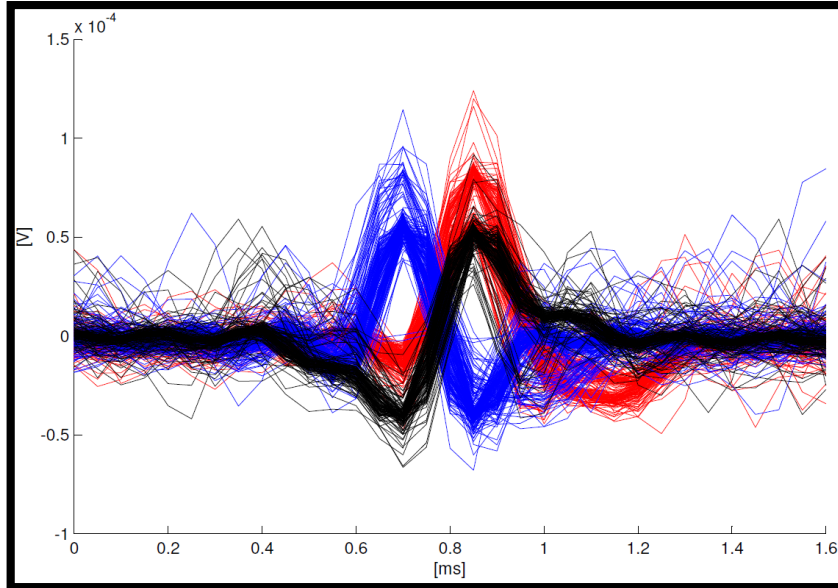


Figure 35. 500 detected, realigned and clustered spikes from a neuronal signal with maximum peak-to-peak voltage of $150 \mu\text{V}$.

5.7 Effectiveness of the Power Supply Filter

In the previous sections, we presented the AFE and the complete signal chain outputs. In order to test the effectiveness of the power supply filter discussed in Section 4.6.1, we carried out a test that was exactly the same as the AFE/signal chain tests, but without the power supply filter. To do so, the output of the power supply filter was shorted out to its input so the passive network was ineffective.

Figure 36 shows the fluctuations on battery voltage when the LEDs are blinking at maximum current. It can be seen that there are very sharp and high-voltage (voltage changes of $\sim 80 \text{ mV}$ in ~ 400 nanoseconds) spikes on the battery voltage. These spikes can easily affect the recorded signal as evident in Figure 37.

In Figure 37, it can be seen that the AFE is working normally. However, there are abrupt fluctuations in the output. This proves that, as expected, the power supply filter removes the high-frequency fluctuations of the power supply rails and is vital to the headstage operation as shown in Section 5.6.

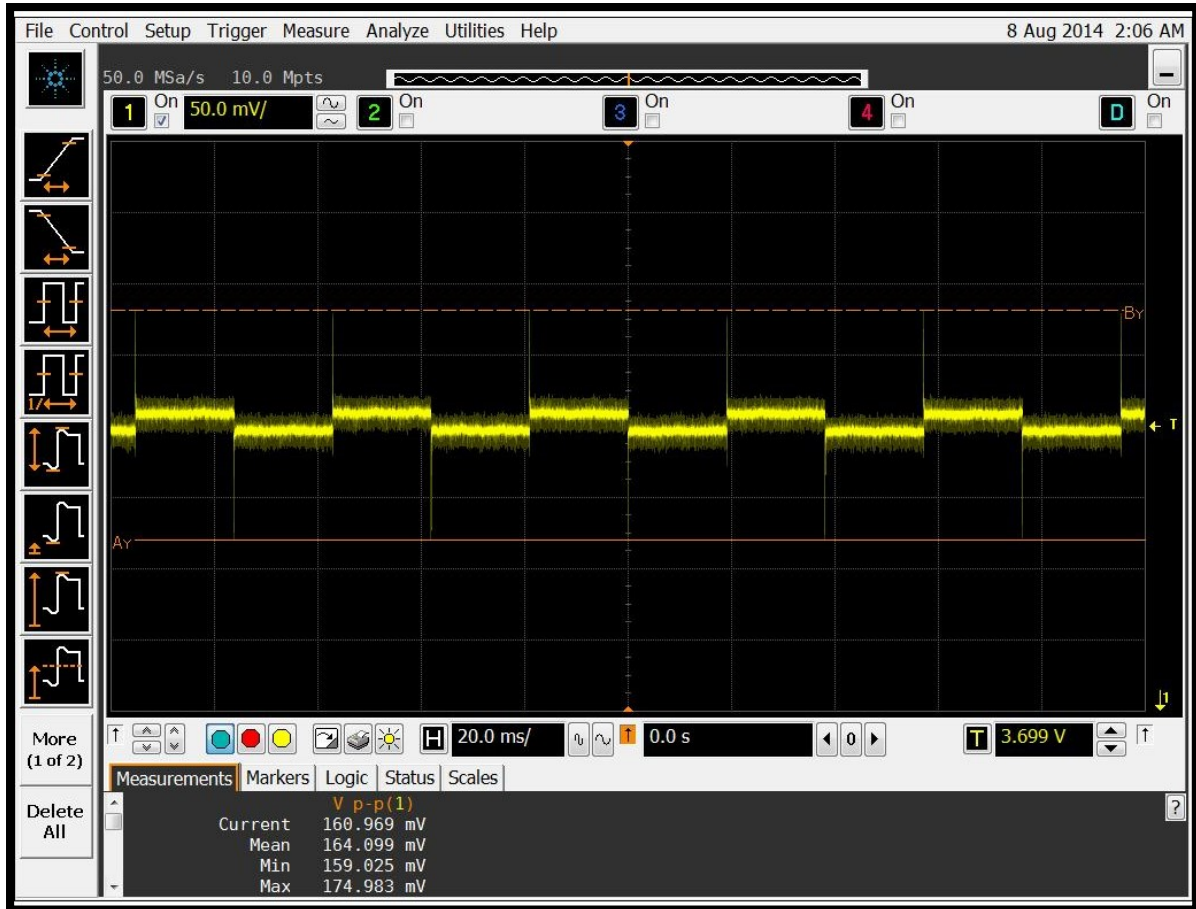


Figure 36. Battery voltage fluctuations when LEDs are blinking at maximum current.

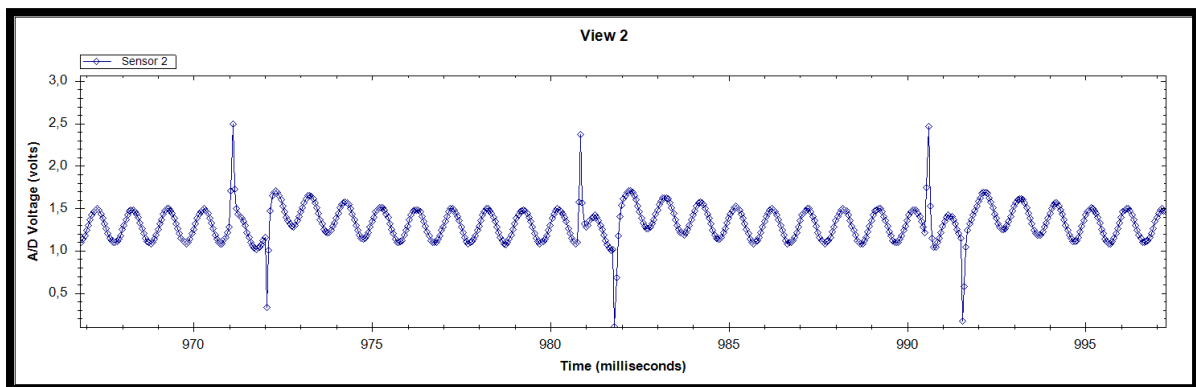


Figure 37. Headstage (signal chain) output without the power supply filter.

5.8 Conclusion

In this chapter, different measured performances of the realized headstage were presented. In this section, we will review the headstage design goals introduced in Chapter 0 and will discuss that these goals have been reached.

5.8.1 Two Optogenetic Stimulation and Recording Channels

In Section 5.4, the voltage waveforms across the LED terminals have been measured and depicted. It can be seen that, when active, the LED voltage is 3.27. This voltage corresponds to a current of 150 mA in the LED [87]. Also, it can be seen in the appendices that there are two LEDs in the designed headstage. Similar to the optical stimulators, the realized headstage has two recording channels and their performance is presented in Section 5.3.

5.8.2 Battery as the Power Source

As evident in sections 4.6 and 5.5, the headstage design is based on a 150 mAh lithium-ion battery. This battery powers the whole system so no power cords are needed.

5.8.3 Optical Stimulation Patterns

In sections 4.5 and 5.4, the design and the measured performance of the optical stimulators were presented, respectively. The high microcontroller clock frequency (compared to the stimulation patterns) and the flexible timer peripherals in the microcontroller result in very accurate control over the generate PWM signals. This is due to the fact that high clock frequency means high time resolution in the microcontroller timers. Figure 30 in Section 5.4 shows the stimulation pattern with the highest frequency. Also, as explained in Section 4.5.1, there is a mechanism available in the headstage that results in very short rise-/fall-times.

5.8.4 Weight and Size Requirements

As discussed in Section 5.2.2, the size of the final headstage rigid-flex PCB (when folded) is less than $20 \times 20 \times 20$ mm³, hence less than the maximum size limit. However, since the final headstage PCB has not been fabricated yet, it is not possible to weight it at this moment. It should be noted that from our previous experience in [17], it is expected that the headstage weight will be satisfying.

Conclusion and Future Works

In this section, we will present the contributions of this work and possible future works that could improve the quality of the wireless optogenetic headstage.

Contributions

The contribution of this work is a novel optogenetic research tool, which allows neuroscientists to perform reliable optogenetic experiments on small rodents. This tool, being a wireless head-mounted device for small animals, has the ability to carry out multi-channel optogenetic stimulation accompanied with simultaneous neural recording. More specifically, this wireless optogenetic headstage is able to stimulate the brain cells using two high-power LEDs and, simultaneously, acquire neural signals from two electrodes samples at 20 kSamples/sec. These features allow researchers to stimulate the brain cell at millisecond scales and investigate the effects of the stimulation in real-time. The optical stimulation patterns created by the high-power LEDs are PWM signals with sharp transients, which in turn adds to the accuracy and usefulness of this device. Also, the analog front end that captures the neural signals has a high robustness against different kinds of noise. Finally, the long life time, the wireless nature, the small size and the low weight of this device allow researchers to carry out long experiments on freely-behaving rodents — a field of study that requires more and more accurate devices to carry more and more sensitive experiments. According to a comprehensive literature review at the time of the writing this thesis, and to the author's knowledge, such optogenetic research tool does not exist in the industry or in the scientific community.

The fact that this headstage fulfills all the requirements is due to experience that was acquired by the author while working on the first version of this wireless headstage. The goal of the mentioned headstage was to have a wireless device that would not need any wires or batteries to operate and would have two electrophysiological recording channels accompanied by one optogenetic stimulation channel. The mentioned optogenetic headstage was powered by an inductive wireless power-delivery link. Many subtle challenges were faced while designing this device and the acquired experience allowed the author to work on the second headstage with confidence.

During the course of this project, the following papers have been published:

- 1) **R. Ameli, A. Mirbozorgi, J.-L. Néron, Y. LeChasseur and B. Gosselin, "A Wireless and Batteryless Neural Headstage with Optical," in Engineering in Medicine and Biology Society (EMBC), Osaka, 2013:** This paper presents the first version of the wireless optogenetic headstage based on which the second headstage was designed. The first version has two recording channels but only one optical stimulation channel and occupies a larger space than the second version. The

power source of this headstage is a wireless power delivery link which can in some scenarios limit the movability of the animal test subjects.

- 2) **S. Mirbozorgi, R. Ameli, M. Sawan and B. Gosselin, "Towards a wireless optical stimulation system for long term in-vivo experiments," in Engineering in Medicine and Biology Society (EMBC), Chicago, 2014:** This paper presents the design of a wireless power delivery chamber where a small rodent can move with a headstage on its head. The headstage can receive its power from the magnetic field generated by the chamber. A power delivery chamber similar to this chamber has been used in the development of the first version of wireless batteryless optogenetic headstage.
- 3) **G. Gagnon-Turcotte, C.-O. Dufresne Camaro, A. Avakh, R. Ameli and B. Gosselin, "A Wireless Multichannel Optogenetic Headstage with on-the-Fly Spike Detection," in International Symposium on Circuits and Systems, Lisbon, 2015:** This paper presents the implementation of a light-weight spike detection algorithm on the wireless headstage that has been developed during this project. The spike detection mechanism is based on the absolute value operator (see section 3.3.2) and it is shown that using real-time spike detection results in reduced power consumption in the wireless transmitter.
- 4) **G. Gagnon-Turcotte, A. Avakh Kisomi, R. Ameli, C.-O. Dufresne Camaro, Y. LeChasseur, J.-L. Neron, P. Brule Bareil, P. Fortier, C. Bories, Y. De Koninck, and B. Gosselin, "A Wireless Optogenetic Headstage with Multichannel Electrophysiological Recording Capability", Sensors, 2015 (Pending review):** This paper presents the research work that has been done in this thesis from the point of view of an electronic designer that aims to design a wireless optogenetic headstage based on COTS components. Desirable characteristics of optogenetic wireless headstages as well as different issues that might be encountered during the design phase and their solutions are also presented in this paper.

Challenges

Similar to the first version of this wireless headstage, many design challenges were face during different design and fabrication phases of this project. The realized wireless headstage consists of analog, digital, RF and mixed-signal subsystems with different requirements that must work simultaneously together. The mixed-signal nature of the headstage, its small form factor and the small power source powering the system, made this project challenging in a multi-disciplinary manner.

The optical stimulation circuitry and the battery had to provide the stimulation LEDs with exactly 150 mA of current. This requirement necessitated LED terminal voltages very close to the battery voltage, which in turn

required a feedback network with very low resistor values — close to the resistance of the PCB tracks. Also the switching behavior of the LEDs resulted in high-amplitude conducted high-frequency and low-frequency noise waveforms on the power rails of the other subsystems.

The problem of switching noise on the power rails manifested itself mostly in the operation of the analog front end — an amplifier with very strict noise characteristics. In order to realize the analog front end with the required noise characteristics, all noise sources must have been identified and taken care of. Four types of noise were present in the analog front end circuitry: 1) the inherent noise of the first-stage amplifier, 2) the common-mode noise at the inputs of the first-stage amplifier, 3) the low-frequency noise on the AFE power rails and 4) the high-frequency noise of the AFE power rails.

The first and second noise sources, pertaining to the first-stage amplifier, were solved by using a low-noise instrumentation amplifier with high CMRR. The low-frequency noise present on the AFE power rails was partially reduced by a passive power supply filter and partially by the high PSRR of the instrumentation and operation amplifiers. Finally, the high-frequency noise of the AFE power rails was filtered out by the power supply filter. It should also be mentioned that the PCB design techniques used in the design of the headstage were also effective in removing different types of noise. Besides the efforts that have been made in the AFE to reduce noise, the use of low noise high-PSRR linear regulators in the power management unit helped with noise problems too. The power management unit consists of two linear regulators with different outputs for different subsystems.

Alongside with the hardware design of the headstage, the firmware design turned out to be challenging too. More specifically, the use of a RTOS to increase the manageability of the code resulted in less CPU time for the useful code. At the same time, the requirements of low power consumption meant lower CPU clock rates so the firmware designer had to make sure that, with the added delays of the RTOS, the code would work perfectly in real-time without losing any packets or data samples.

Last but not least, the PCB design of the final headstage required very careful component placement and even floor planning ahead of the placement process as the PCB size had to be small in comparison with a rodent body. Also, the small form factor of the PCB and the EMC/EMI issues that would exist without careful PCB design made the design challenging above the challenges of the circuit design. To address all the EMC/EMI issues, a six-layer flex-rigid PCB technology was adopted and allowed us to find a solution to all design problems.

The headstage system, after design and fabrication, went through different types of test that covered the functionality of the AFE, the optical stimulation circuitry, the MPU and the radio transceiver. In these tests the